Simulation of Ternary Mixtures of Ethylene, 1-Hexene, and Polyethylene

Shyamal K. Nath,† Brian J. Banaszak, and Juan J. de Pablo*

Department of Chemical Engineering University of Wisconsin−Madison, Madison, Wisconsin 53706

Received December 27, 2000; Revised Manuscript Received June 20, 2001

ABSTRACT: Solubility and diffusion of ethylene and 1-hexene mixtures in linear amorphous polyethylene (modeled as C_{70}) are studied using a recently proposed united atom force field. It is found that the presence of 1-hexene increases the solubility of ethylene in polyethylene. These results are also compared to the solubility predictions of the SAFT equation of state. It is also observed that, in the polymer phase, both ethylene and 1-hexene molecules prefer to reside in the vicinity of the polymer chain ends. This aggregation effect may be important in determining penetrant solubilities in longer polymers and polymers with short chain branches.

1. Introduction

In the commercial gas-phase manufacture of linear low-density polyethylene, a higher α-olefin, typically 1-butene, 1-hexene, or 1-octene, is used as a comonomer; a ternary mixture of ethylene, α-olefin, and polyethylene therefore coexist in the reactor during polymerization. To develop a sound understanding of the kinetics of polymerization processes, and hence the quality of the product resin, precise knowledge of the solubility and diffusion of ethylene and the α-olefin in polyethylene is required at reaction conditions. Solubility data are required for design of polymerization reactors as well as devices for safe handling of the reaction products. Experimental studies of sorption of multicomponent gas mixtures in polyolefins under reactor conditions are expensive and time-consuming. Furthermore, safety considerations can add significantly to the cost of such work. Practical industrial applications have traditionally relied on empirical correlations and semitheoretical equations-of-state to generate solubility information on such solutes and their mixtures in relevant polymeric systems.

In a previous study,[1] we have shown that several, widely used equations-of-state fail to provide high-accuracy predictions of phase equilibria for binary polyolefin mixtures (particularly mixtures of highly asymmetric components such as ethylene, C_{40}). In contrast, when a suitable molecular force field is available, molecular simulations have been shown to constitute a valuable predicting tool for such calculations.[1,2]

With the advent of novel Monte Carlo techniques such as the Gibbs ensemble,[3,4] configurational-bias methods,[5,6] and expanded-ensemble methods,[7] it is now possible to use molecular simulations to generate phase diagrams for mixtures of moderately long molecules with relative ease. Interestingly, even though the extension of the Gibbs ensemble technique to simulate ternary mixtures is straightforward, only a few simulation studies exist for phase equilibria of ternary systems involving long alkanes.[2,8] Prior to our recent study of ternary mixtures of polyethylene with solutes such as nitrogen, methane, and ethane,[2] most simulation studies of ternary mixtures had been limited to mixtures of simple molecules.[8,9] More recent articles explore phase equilibria for *n*-alkanes.[10,11]

Knowledge of ternary phase equilibria for alkane systems is important in both the polymer and the petrochemical industries. Considering the chemical simplicity that characterizes such systems, molecular simulations could provide a useful tool to understand and determine the phase behavior of these systems. Furthermore, simulations could provide molecular level insights into the complicated phase behavior of these systems. In previous work,[2] we studied the solubility of gaseous mixtures of small molecules (e.g., methane, nitrogen, ethane) in a polymer for several systems of engineering importance. In this work, we study the solubility of ethylene−1-hexene gas mixtures in linear amorphous polyethylene, modeled as C_{70}, under conditions of importance to the polyethylene manufacturing industry.

The paper is organized as follows. We begin with a brief description of the model and simulation methods employed to generate phase diagrams. We then provide a brief description of the SAFT equation-of-state model employed to generate phase equilibrium predictions. Next, we present results for pure 1-hexene simulations. Then, we present solubility results for ethylene−1-hexene mixtures in C_{70} at various conditions. To understand the relative diffusion of ethylene and 1-hexene molecules in their ternary mixture with polyethylene, we also conduct diffusion calculations at one state condition. We then analyze solute−solute and polymer−solute intermolecular correlation functions. We conclude with a few remarks concerning the solubility of small molecules in polymers and the possibilities of molecular simulations in regard to the study of realistic mixtures of industrial interest.

2. Simulation Details

A united-atom representation of the alkanes and the alkenes is adopted throughout this work. A list of the intra- and intermolecular force field parameters adopted in this work for C_{70}, ethylene, and 1-hexene is provided in Tables 1 and 2. A Lennard-Jones potential energy function is adopted to describe site−site interactions

† Current address: Accelrys Incorporated, 9685 Scranton Road, San Diego, CA 92121.

* To whom correspondence should be addressed.

10.1021/ma002197l CCC: $20.00
Published on Web 09/19/2001

Table 1. Intramolecular Potential Energy Functions

Bond Stretching Potential	
$V(r)/k_B = (K_r/2)(r - b_{eq})^2$	$b_{eq} = 1.54$ Å (C−C)
$K_r = 96500K/Å^2$	$b_{eq} = 1.34$ Å (C=C)
Bond Bending Potential	
$V(\theta)/k_B = (K_\theta/2)(\theta - \theta_{eq})^2$	$\theta_{eq} = 114.0°$ (C−C−C)
$K_\theta = 62500K/rad^2$	$\theta_{eq} = 124.0°$ (C−C=C)
Torsional Potential	
$V(\phi)/k_B = V_0 + V_1(1 + \cos\phi) + V_2(1 - \cos 2\phi) + V_3(1 + \cos 3\phi)$	
C−C−C−C	
$V_0 = 0$	$V_1 = 355.04K$
$V_2 = -68.19K$	$V_3 = 791.32K$
C−C−C=C	
$V_0 = 685.96K$	$V_1 = 86.31K$
$V_2 = -109.71K$	$V_3 = 282.08K$

Table 2. Intermolecular Potential Energy Functions

Nonbonded Interaction Potential	
$V(r) = 4\epsilon[(r/\sigma)^{12} - (r/\sigma)^6]$	
C_{70}	
$\sigma_{CH_2(sp^3)} = 3.93$ Å	$\epsilon_{CH_2(sp^3)} = 45.8K$
$\sigma_{CH_3(sp^3)} = 3.91$ Å	$\epsilon_{CH_3(sp^3)} = 104.0K$
Ethylene	
$\sigma_{CH_2(sp^2)} = 3.79$ Å	$\epsilon_{CH_2(sp^2)} = 84.7K$
1-Hexene	
$\sigma_{CH_3(sp^3)} = 3.78$ Å	$\epsilon_{CH_3(sp^3)} = 113.0K$
$\sigma_{CH_2(sp^2)} = 3.72$ Å	$\epsilon_{CH_2(sp^2)} = 96.5K$ (end group)
$\sigma_{CH_2(sp^3)} = 3.93$ Å	$\epsilon_{CH_2(sp^3)} = 45.8K$ (middle group)
$\sigma_{CH(sp^2)} = 3.85$ Å	$\epsilon_{CH(sp^2)} = 39.7K$

both for sites located more than three bonds apart (on the same molecule) and sites located on different molecules. For both the alkanes and the alkenes, a torsional potential energy function is also imposed on rotations about carbon−carbon bonds.[12] Bond stretching and bond angle bending are manipulated by means of a harmonic potential. For nonbonded, unlike pair interactions, we use Lorentz−Berthelot combining rules, which in previous work have been shown to be suitable for alkane mixtures.[1] In all calculations, a cutoff radius of 10.0 Å is employed for Lennard-Jones interactions, and standard tail corrections[13,14] are implemented.

For both the alkanes and ethylene, we use the recently proposed NERD force field[15,16] for the intra- and intermolecular force field parameters. The NERD force field has been shown to provide good agreement with experimental phase equilibria data for pure alkanes and their binary and ternary mixtures.[1,2]

An independent set of parameters is adopted for 1-hexene. The parameters for 1-hexene were determined by a slight modification of the parameters for alkanes, as to agree with the orthobaric densities for 1-hexene. The 1-hexene CH_2 end group of sp^2 hybridization differs from the ethylene CH_2 end group of sp^2 hybridization because the two types are bonded to two different site types; the ethylene CH_2 end group is bonded to another CH_2 end group, and the 1-hexene CH_2 end group is bonded to a CH group of sp^2 hybridization. The parameters for the C_{70}, CH_3 end group are from the generalized NERD force field,[15] while the parameters for the 1-hexene CH_3 end group of sp^3 hybridization were determined as to reproduce the orthobaric densities for 1-hexene. Since the time of this work, a more consistent force field has been developed for α-olefins.[16] We note, however, that results for a few select conditions yield identical results for the two force fields.

For pure 1-hexene, phase equilibria simulations were conducted in the Gibbs ensemble, at constant volume and temperature.[3] Vapor pressures for 1-hexene where calculated by evaluating the pressures from a constant NVT molecular dynamics simulation at the coexistence vapor density obtained from coexistence calculations. For mixtures, all phase equilibria simulations were conducted in the Gibbs ensemble, at constant pressure and temperature.[4]

A general Gibbs ensemble consists of two simulation boxes at coexistence; the two boxes are at the same temperature, pressure, and chemical potential for each species. In this work, the two boxes represent a polymer phase and a vapor phase. The criteria for phase equilibria are met by three types of moves: random displacements of molecules in each box at constant volume, random changes of the volume in each box, and trial particle exchanges between the two boxes. More information can be found in earlier references.[3,4]

In all our simulations, constant volume molecule displacements are conducted by means of a hybrid Monte Carlo (HMC) procedure.[17,18] In the HMC procedure, five molecular dynamics steps were used to generate a global trial Monte Carlo move. As part of the HMC procedure, a time step of 2.0 ps was used for the molecular dynamics trial moves.

Volume displacements generate trial configurations by randomly displacing the size of the box by a maximum of 2% and by rescaling the center-of-mass for each molecule; the molecular structure of each molecule does not change during the move.

For a polymer−small molecule mixture at low to moderate pressures, the vapor phase is polymer-free. To increase efficiency, trial attempts to transfer the polymer molecules from the polymer phase to the vapor phase are rejected during those simulations. In a previous study, we have seen that such rejection does not affect the simulation results appreciably.[2]

To generate phase equilibria data that are useful for reactor design, simulations of solubility must be carried out at a specified gas-phase composition. Gibbs ensemble simulations of that nature, however, are difficult without prior knowledge of the relative composition of the solvents in the polymer phase. To obtain a rough estimate of the polymer-phase composition, short preliminary simulations are performed before starting an actual production run.

In this study, we model amorphous polyethylene as linear alkane chains of 70 carbon units. In conducting all the simulations, we restricted our system to 10 polyethylene chains (of 70 segments each). The number of solvent particles was adjusted so that the simulation box size of the gas phase was always slightly larger than that of the polymer phase. The average number of small molecules present in the polymer phase in a binary ethylene−C_{70} mixture at 85°*C* and 150 psia is in the range of 6−11. For ternary mixtures of ethylene, 1-hexene, and C_{70}, the number of solvent molecules in the polymer-rich phase ranges from 7 to 12 for ethylene and 30−36 for 1-hexene, when the partial pressure of ethylene is 153.3 psia and that of 1-hexene is 16.7 psia, at 85 °C. Equilibrium averages were collected for about 3×10^7 simulation steps, of which 5% were volume moves, 5−10% were HMC moves, and the rest were transfer moves.

3. SAFT Equation-of-State

For the systems studied in this work we also conduct equation-of-state predictions using the SAFT model.

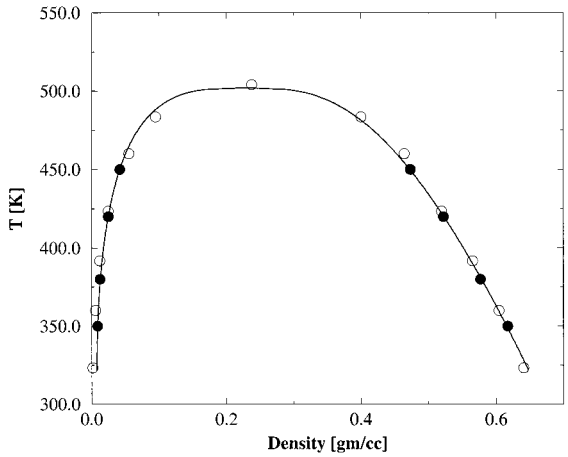

Figure 1. Orthobaric densities for 1-hexene. The filled circles are simulation results from present work, the open symbols are experimental results,[26] and the lines show an Ising fit to the simulation points. The error bars near the critical point are less than 3 times the size of the symbols. Error bars at lower temperatures are less than twice the size of the symbols.

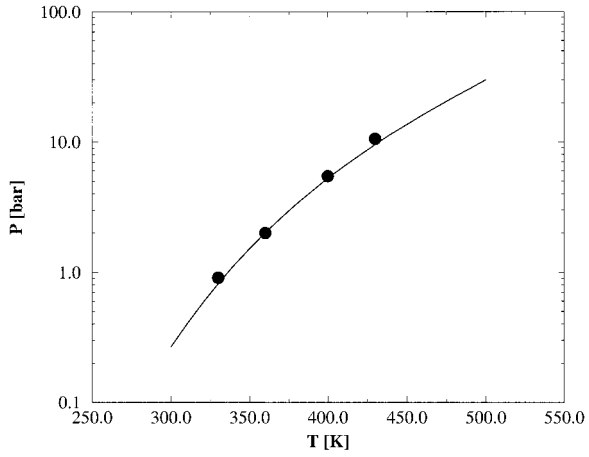

Figure 2. Saturation pressures for 1-hexene. The filled circles are simulation results from the present work, and the curves are from experimental correlations.[27] The error bars for vapor pressure of the present work are about one symbol size.

Such a model has been widely used to correlate experimental phase equilibrium data for polymer−solvent systems; it is therefore of interest to compare its predictions to those of simulations.

The SAFT compressibility factor is assumed to consist of the sum of several contributions, that is

$$Z = Z(\text{reference}) + Z(\text{chain}) + Z(\text{association}) \quad (1)$$

where the term $\boldsymbol{Z}$(reference) corresponds to a reference system of spherical sites (e.g., hard sphere plus a dispersion term). The term $\boldsymbol{Z}$(chain) describes the effect of bonding of spherical sites to form chains, and the term $\boldsymbol{Z}$(association) is introduced to account for association between nonbonded sites. Detailed expressions for each of the terms in eq 1 can be found in the original references.[19−21] For mixtures, rigorous statistical-mechanical expressions are used to describe the hard-sphere, chain, and association terms: an empirical mixing rule is needed, however, for the dispersion term (e.g., a volume fraction approximation).

The substance-specific parameters appearing in SAFT are found in the original references. For ethylene and 1-hexene, the tabulated values are used. Published correlations are used to extrapolate substance-specific parameters for C_{70}. In this work, the binary interaction parameter is set to zero for all SAFT solubility predictions.

4. Results and Discussion

4.1. 1-Hexene Simulations. Figure 1 shows experimental and simulated orthobaric densities for 1-hexene using the parameters shown in Tables 1 and 2. In Figure 1, the open circles correspond to experimental data, and the filled circles are results from the current simulations. To complete the coexistence curves near the critical point, we fit the results of simulations to a simple Ising scaling-law analysis using a critical exponent $\beta = 0.32$;[22] as we are mainly interested in the phase behavior of alkenes away from the critical point, no crossover or finite-size corrections were implemented in this work to estimate critical properties. The Ising fit curve is also shown in Figure 1 by a solid line. Figure 1 shows that simulation results for 1-hexene are in good agreement with experimental data. Another important test for molecular models is their ability to correctly describe the vapor pressure. Figure 2 shows simulated and experimental vapor pressures of 1-hexene at different temperatures. Agreement between experiment and simulation is satisfactory.

4.2. Solubility. Phase equilibria simulations for ternary ethylene, 1-hexene, and amorphous polyethylene (C_{70}) are conducted at three temperatures, 65, 85, and 105 °C, and at various partial pressures of the solvent ethylene and 1-hexene molecules. We first simulate the solubility of pure ethylene in C_{70} at all three temperatures and at pressures of 100, 150, and 200 psia, respectively. These binary simulations correspond to results at zero 1-hexene partial pressure. We then add 1-hexene molecules to the simulation boxes and conduct calculations with 1-hexene partial pressures of up to about 20 psia.

In our ternary mixture simulations, we are interested in generating data at fixed partial pressures of ethylene and 1-hexene. However, since we use a Gibbs ensemble, we can only control the total pressure, and consequently, our results are only within 5% of the target ethylene partial pressure.

Figure 3 shows the simulation and SAFT predictions for the solubility of pure ethylene at the three different temperatures and at various pressures. The symbols correspond to the simulation results, and the lines correspond to the predictions from the SAFT equation-of-state. The simulated solubility of ethylene increases with decreasing temperature; at 65 °C, it is considerably higher than at 85 °C, and and at 85 °C, the ethylene solubility is considerably higher than at 105 °C. These observations are consistent with the available experimental data for solubility at higher temperatures. In previous work,[1] we also compared simulated Henry's constants for ethylene in polyethylene between 150 and 400 °C (with the NERD force field) and found excellent agreement with available experimental data.

From the results in Figure 3, we find that solubility increases in a linear fashion with increasing pressure at all three temperatures. The linear increase in the solubility demonstrates that, within the limit of our simulation pressures for the binary mixtures, Henry's law behavior is obeyed. From our simulation results, approximate weight fraction Henry's constants for ethylene in polyethylene are 531, 586, and 999 bar at 65,

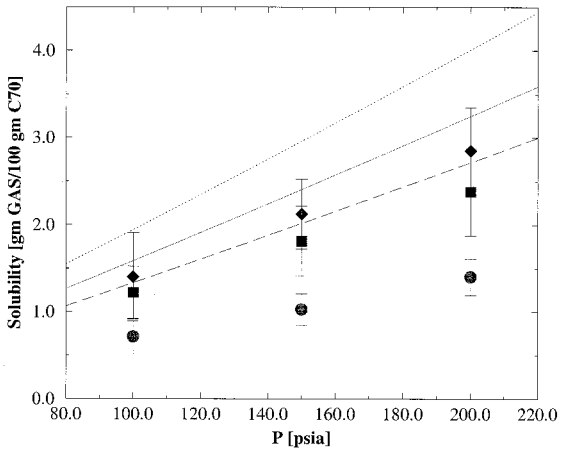

Figure 3. Solubility of ethylene in C_{70} as a function of pressure. The symbols correspond to the results of our simulations. The circles correspond to solubility data at 105 °C, the squares correspond to solubility data at 85 °C, and the diamonds correspond to solubility data at 65 °C. The lines correspond to predictions of SAFT. The long-dashed line corresponds to SAFT predictions at 105 °C, the solid line corresponds to SAFT predictions at 85 °C, and the short-dashed line corresponds to SAFT predictions at 65 °C. The error bars are the standard deviations of solubility block averages. Each block length is set to one correlation time.

85, and 105 °C, respectively. SAFT also predicts Henry's law behavior within the simulation pressures, with approximate weight fraction Henry's constants for ethylene in polyethylene of 359, 440, and 522 bar at 65, 85, and 105 °C, respectively. As can be seen, SAFT predictions overpredict the simulation solubility results by 30−50%. This is consistent with previous studies where it has been observed that, without adjusting the binary interaction parameter, SAFT fails to accurately predict experimental and simulation results for mixtures of ethylene and long alkanes.[1]

Figure 4 shows simulation and SAFT predictions for the solubilities of ethylene and 1-hexene in ternary mixtures with C_{70} at 65 °C and three different partial pressures of ethylene, namely 100, 150, and 200 psia. Results are shown for various partial pressures of 1-hexene. The simulation data in Figure 4 show that, for a fixed ethylene partial pressure, the solubilities of ethylene and 1-hexene increase when the 1-hexene partial pressure increases. For 1-hexene, the solubility remains unchanged with an increase of the ethylene partial pressure. The SAFT model predicts the same trends as the simulations, but it overpredicts ethylene solubilities by about 30% for all three ethylene partial pressures. Also, SAFT predicts a greater change in ethylene solubility due to the change in ethylene partial pressure than the simulations. For 1-hexene solubilities, the SAFT predictions appear to be in close agreement with the simulation results at low 1-hexene partial pressures, but SAFT overpredicts simulated 1-hexene solubilities at higher 1-hexene partial pressures.

Figure 5 shows simulation and SAFT predictions for solubilities of ethylene and 1-hexene in ternary mixtures with C_{70} at 85 °C and three different partial pressures of ethylene (100, 150, and 200 psia). Results are shown for various partial pressures of 1-hexene. We find results analogous to those for the solubility of ethylene at 65 °C; i.e., for a fixed ethylene partial pressure the solubility of ethylene increases with increasing 1-hexene partial pressure. For 1-hexene, the solubility remains

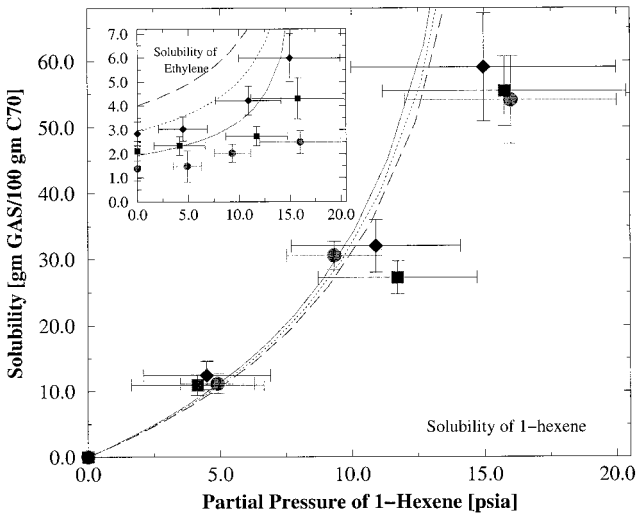

Figure 4. Solubility of the solutes in C_{70} at 65 °C. Solubility of 1-hexene is presented in the main frame, and solubility of ethylene is presented in the inset. The symbols correspond to the results of our simulations. The circles correspond to an ethylene partial pressure of 100 psia, the squares correspond to an ethylene partial pressure of 150 psia, and the diamonds correspond to an ethylene partial pressure of 200 psia. The lines correspond to predictions of SAFT. The solid line corresponds to SAFT predictions at an ethylene partial pressure of 100 psia, the short-dashed line corresponds to SAFT predictions at an ethylene partial pressure of 150 psia, and the long-dashed lines correspond to SAFT predictions at an ethylene partial pressure of 200 psia. The error bars are the standard deviations of solubility and 1-hexene pressure block averages. Each block length is set to one correlation time.

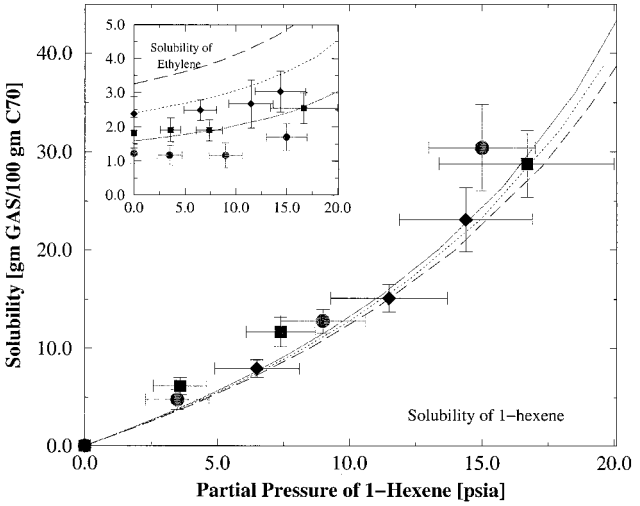

Figure 5. Solubility of the solutes in C_{70} at 85 °C. Solubility of 1-hexene is presented in the main frame, and solubility of ethylene is presented in the inset. The meanings of the symbols, lines, and error bars are the same as Figure 4.

unchanged with an increase in ethylene partial pressure. The SAFT predictions are similar to the 65 °C case. The predictions follow the same trends as the simulation results, but they overpredict ethylene solubilities; they also predict a greater dependence of solubility on ethylene partial pressure. The SAFT 1-hexene solubility predictions appear to be in close agreement with the simulation results.

Figure 6 shows simulation and SAFT predictions for solubilities of ethylene and 1-hexene in ternary mixtures with C_{70} at 105 °C and three different partial pressures of ethylene, 100, 150, and 200 psia, and at various

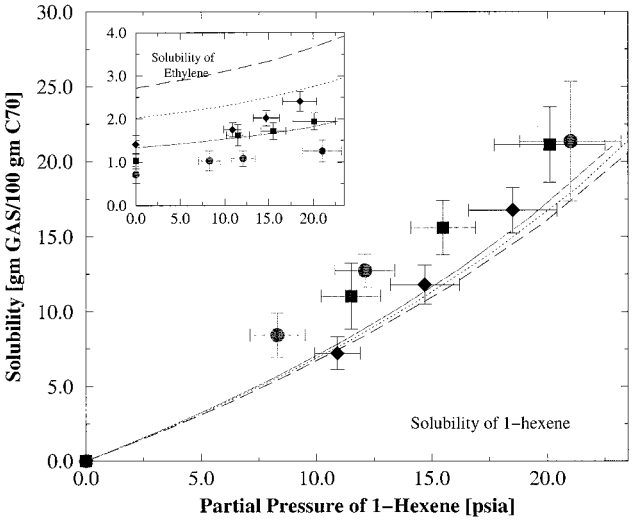

Figure 6. Solubility of the solutes in C_{70} at 105 °C. Solubility of 1-hexene is presented in the main frame, and solubility of ethylene is presented in the inset. The meanings of the symbols, lines, and error bars are the same as Figure 4.

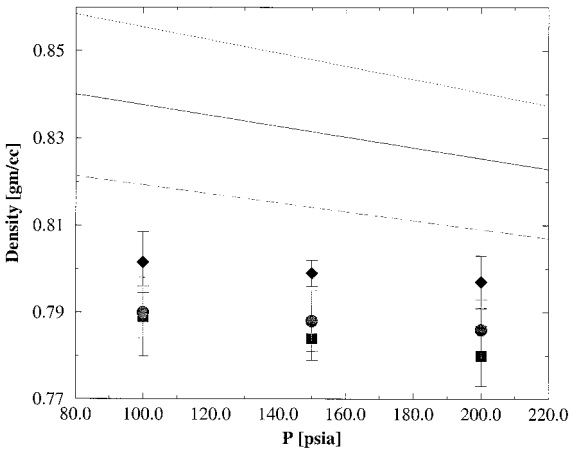

Figure 7. Density of the polymer phase in the binary mixture of ethylene and C_{70}. The meaning of the symbols and lines are as in Figure 3. The error bars are the standard deviations of density block averages. Each block length is set to one correlation time.

partial pressures of 1-hexene. As before, we find that for a fixed ethylene partial pressure the solubility of ethylene increases with an increase in 1-hexene partial pressure. For 1-hexene, solubility decreases slightly with an increase in ethylene partial pressure. The SAFT predictions are analogous to those for lower temperatures. The ethylene solubility SAFT predictions overpredict the simulation solubilities and overpredict the simulation results for the effect of ethylene partial pressure on ethylene solubility. However, the SAFT predictions for ethylene solubilities do follow the same trends as the simulation results. For 1-hexene, SAFT predicts similar solubilities as the simulations; it also predicts that 1-hexene solubility should decrease slightly with an increase in ethylene partial pressure.

Simulation and SAFT predictions for the densities of the polymer-rich phases are shown in Figures 7−10. Figure 7 shows the density of the polymer-rich phase from binary ethylene−C_{70} simulations and SAFT predictions. The simulations show that density increases with an increase in temperature and decreases with an increase in ethylene partial pressure. This is due to the

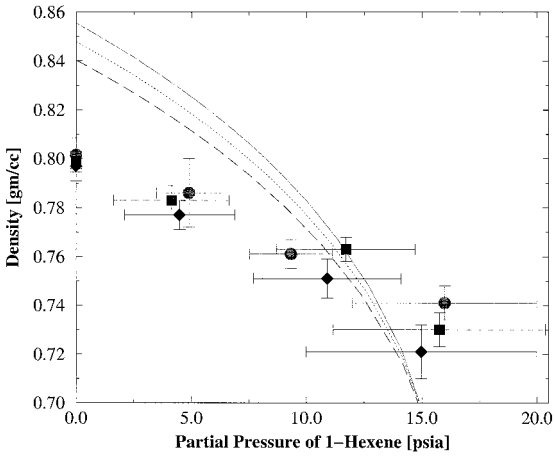

Figure 8. Density of the polymer phase in the ternary mixture of ethylene, 1-hexene. and C_{70} at 65 °C. The meaning of the symbols and lines are as in Figure 4. The error bars are the standard deviations of density and 1-hexene pressure block averages. Each block length is set to one correlation time.

fact that both an increase in temperature as well as a decrease in ethylene partial pressure reduce the concentration of ethylene in C_{70}. SAFT predicts similar trends as the simulations. However, SAFT densities are about 3−7% higher than the simulation results. According to SAFT, densities exhibit a larger dependency on temperature than that estimated by simulations.

The density behavior of the polymer-rich phase in a ternary ethylene, 1-hexene, and C_{70} mixture is more complicated than that in the binary mixtures. Figures 8, 9, and 10 show simulation and SAFT predictions for the densities of ternary mixtures at 65, 85, and 105 °C, respectively. For the simulations, the general trend from the figures is that an increase in the 1-hexene partial pressure decreases the density of the polymer-rich phase. This observation is consistent with the observation in Figure 7. SAFT predicts the same trends as the simulations. However, as in the binary mixture case, SAFT overpredicts the simulated densities of the polymer-rich phase.

4.3. Diffusion. Diffusion coefficients are determined from the mean-squared displacement

$$D = (1/6t)\langle|\boldsymbol{r}(t) - \boldsymbol{r}(0)|^2\rangle \qquad (2)$$

where $\boldsymbol{r}(t)$ denotes the coordinates of the center-of-mass of the molecules at time (t). We use a constant NVT molecular dynamics simulation to generate the coordinates. The density and the composition are fixed at the values corresponding to the Gibbs ensemble simulation results for a given pressure and temperature of the system. A simple Nosé−Hoover thermostat[23] is implemented to control the temperature of the system during the simulation.

In this work we were only interested in the relative diffusion of ethylene and 1-hexene in their ternary mixture with C_{70}. The system we study here is at 85 °C with an ethylene partial pressure of 153.3 psia and 1-hexene partial pressure of 16.7 psia. The total density for this system is 0.746 g/cm^3, and the mole fractions for ethylene and 1-hexene are 0.17 and 0.64, respectively. Figure 11 shows average mean-square displacements for an ethylene and a 1-hexene molecule in C_{70} in a log−log plot. The irregularity of the mean-square-displacement for 1-hexene at long times (1000−3000 ps) is noise due to limited sampling at such time scales.

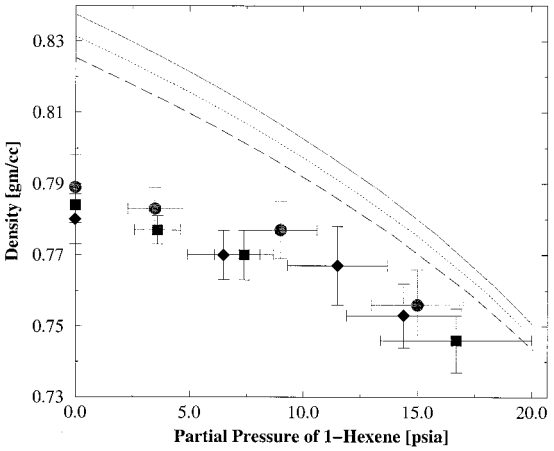

Figure 9. Density of the polymer phase in the ternary mixture of ethylene, 1-hexene, and C_{70} at 85 °C. The meaning of the symbols and lines are as in Figure 4. The error bars are as in Figure 8.

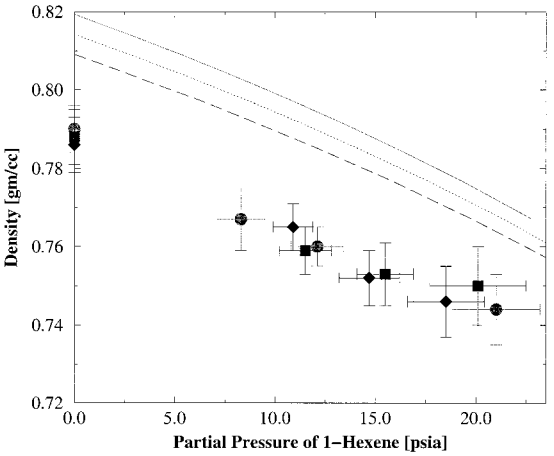

Figure 10. Density of the polymer phase in the ternary mixture of ethylene, 1-hexene, and C_{70} at 105 °C. The meaning of the symbols and lines are as in Figure 4. The error bars are as in Figure 8.

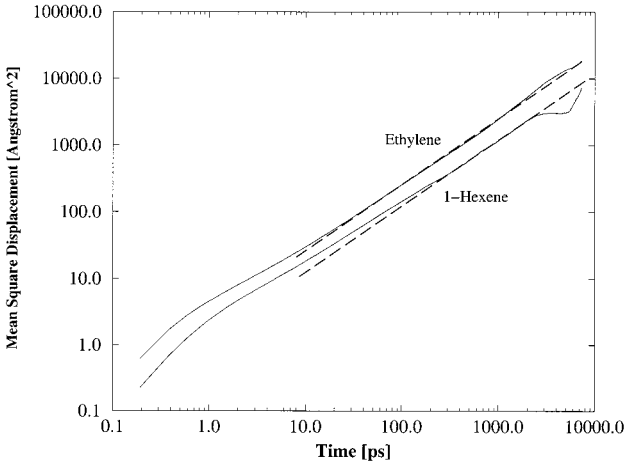

Figure 11. Mean-square displacement vs time curves in log–log representation for ethylene and 1-hexene at 85 °C at ethylene partial pressure of 153.3 psia and 1-hexene partial pressure of 16.7 psia. The dashed lines correspond to lines with unit slope.

Previous studies[24] have pointed out that long molecular dynamics simulation runs are required to obtain the linearity of the mean-square displacement vs time curves. In our previous work on HALS diffusion in polyethylene[18] we obtained simulation trajectories of about 30 ns. In this work it is sufficient to generate the mean-square displacement curves from simulation trajectories of about 10 ns.

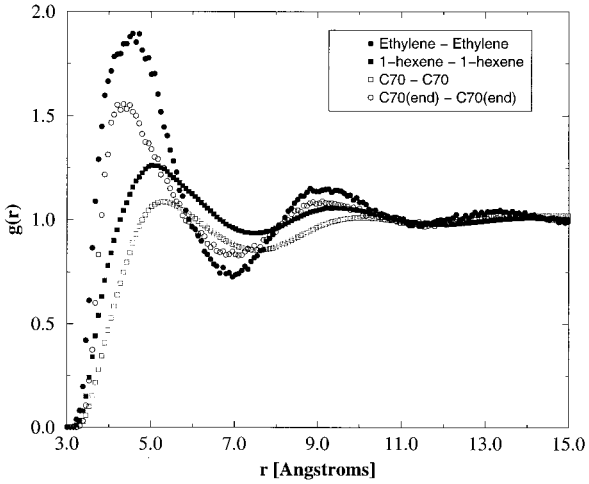

Figure 12. Site–site self-intermolecular pair correlation functions for ethylene, 1-hexene, C_{70}, and C_{70}(end) sites in a ternary mixture at 85 °C with an ethylene partial pressure of 153.3 psia and 1-hexene partial pressure of 16.7 psia. The correlation functions for ethylene, 1-hexene, and C_{70} include the site interactions for all sites in each molecule. The correlation function for C_{70}(end) includes only the methyl groups at the end of the C_{70} chains.

The calculated diffusion coefficients corresponding to Figure 11 are $(4.36 \pm 0.90) \times 10^{-5}$ and $(2.00 \pm 0.40) \times 10^{-5}$ cm^2/s for ethylene and 1-hexene, respectively. The diffusion coefficient for ethylene is about 2.2 times larger than that of 1-hexene, which is consistent with their size differential.

4.4. Pair Correlation Functions. Some interesting features are revealed by the solute–solute and solute–polymer intermolecular pair correlation functions of the ethylene, 1-hexene, C_{70} ternary mixture. All the pair correlation functions presented in this section correspond to the ternary system at 85 °C and the same conditions used for diffusion studies. Figure 12 shows self-intermolecular pair correlation functions; the filled circles correspond to ethylene–ethylene, the filled squares correspond to 1-hexene–1-hexene, the open squares correspond to C_{70}–C_{70}, and the open circles correspond to C_{70} end group–C_{70} end group pair correlation functions. The C_{70}–C_{70} function represents correlations between any site of a C_{70} molecule, whereas the C_{70} end group–C_{70} end group function represents correlations between end groups of the C_{70} chains only.

Of all the self-intermolecular pair correlation functions in Figure 12, the ethylene–ethylene function has the largest first peak. It is interesting to observe the strength of the C_{70} end group–C_{70} end group pair correlation function, which has a much larger first peak compared to the C_{70}–C_{70} function. The larger first peak implies that the end sites prefer themselves over an average C_{70} site.

Figure 13 represents ethylene pair correlation functions with ethylene, 1-hexene, C_{70}, and C_{70} end groups. The first peak of the ethylene–ethylene pair-correlation function is large and has a much higher value than that of the ethylene–C_{70} function. A stronger first peak for the ethylene–ethylene interaction indicates that ethylene molecules prefer to stay close to each other and form "aggregates" when dissolved in C_{70}. Another

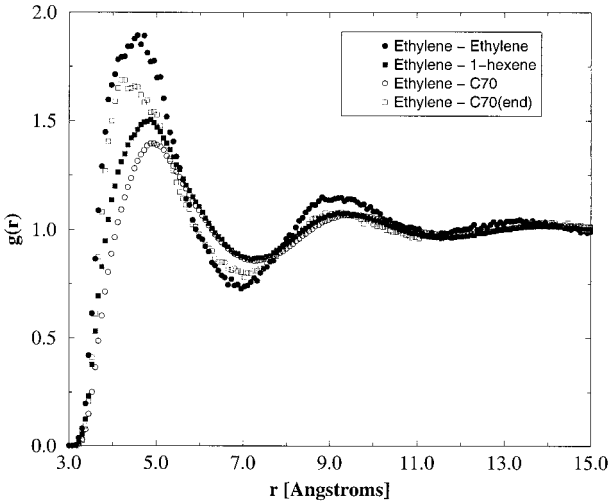

Figure 13. Site−site intermolecular pair correlation functions for ethylene sites in a ternary mixture at 85 °C with an ethylene partial pressure of 153.3 psia and 1-hexene partial pressure of 16.7 psia. The correlation functions are the same as in Figure 12.

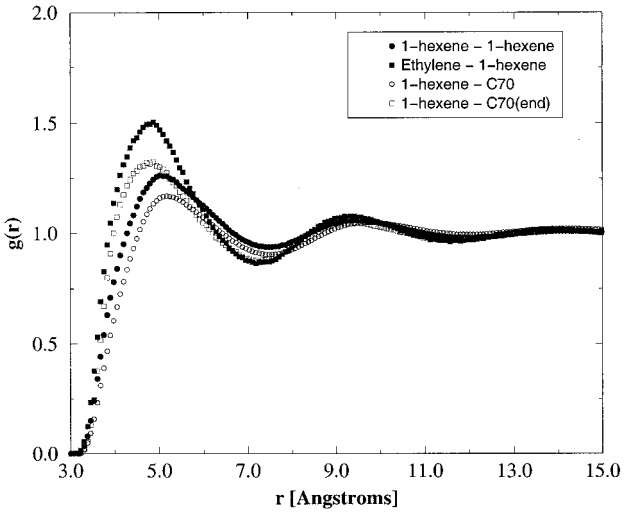

Figure 14. Site−site intermolecular pair correlation functions for 1-hexene sites in a ternary mixture at 85 °C with an ethylene partial pressure of 153.3 psia and 1-hexene partial pressure of 16.7 psia. The correlation functions are the same as in Figure 12.

observation from Figure 13 pertains to the relative strength of the first peak of the ethylene−C_{70} and the ethylene−C_{70} end group correlations. The first peak of the ethylene−C_{70} end group function is higher than that of the ethylene−C_{70}, indicating that ethylene aggregates prefer to reside near the end sites of the C_{70} chains. This observation is in good agreement with our previous studies of the methane−ethane−polyethylene system,[2] where we found that solute particles prefer to aggregate near end sites of the polymer chains. It is also interesting to point out that the ethylene−C_{70} end group correlation is also stronger than the ethylene−1-hexene function. From an entropic point of view, because the C_{70} end sites are only bonded to one other site instead of two other sites (like the other 68, C_{70} sites), they will be surrounded by more available volume. Therefore, C_{70} end sites will have a tendency to "attract" small ethylene aggregates.

Figure 14 shows 1-hexene intermolecular pair-correlation functions with ethylene, 1-hexene, C_{70}, and C_{70} end groups. In contrast to ethylene functions, the 1-hexene−1-hexene function is only barely more pronounced than the 1-hexene−C_{70} function. This implies that, for 1-hexene, the tendency to form aggregates in the polymer is very weak. However, we also conclude from Figure 14 that 1-hexene molecules prefer to stay close to an ethylene molecule or the end sites of the C_{70} chains in the ternary mixture for the same entropic reasons already stated.

Figures 12 and 13 would suggest that a cutoff radius of 10.0 Å for Lennard-Jones interactions may be too short because the intermolecular pair-correlation functions are not exactly unity at this distance. This effect is most pronounced for the ethylene−ethylene pair correlation. A cutoff radius of 10.0 Å corresponds to 2.6 times the ethylene Lennard-Jones size parameter (σ_{CH_2} = 3.79 Å for ethylene). We have performed several simulations with longer cutoffs (as high as 13 Å), and we find that our results are identical to those obtained with a 10 Å cutoff.

5. Conclusions

Monte Carlo simulations with a Gibbs ensemble method have been conducted to study the solubility of mixtures of ethylene and 1-hexene in C_{70}. A recently proposed united-atom force field was used for this study. This force field has been tested for binary and ternary[1,2] mixtures of small molecules with long alkanes previously and has been shown to work well in comparison to experimental data for those systems. Results of simulations show that, within the range of simulation pressures and temperatures, the solubility of pure ethylene could be approximated with Henry's law. From the simulation of ternary mixtures, we can conclude that the presence of 1-hexene molecules slightly increases the solubility of ethylene in polyethylene.

The simulation results were compared with predictions from the SAFT equation-of-state. We find that SAFT predicts the same general trends as the simulation results. However, SAFT appears to overpredict ethylene solubilities and mixture densities as compared to the simulation results. Also, SAFT appears to overpredict the ethylene solubility dependency on ethylene partial pressure for the ternary mixtures and the temperature dependency of the binary mixture densities as compared to the simulations. This is consistent with a previous study on the predictive capabilities of SAFT.[1]

The diffusion of ethylene and 1-hexene in C_{70} in their ternary mixture is also studied. From our simulations we find that the diffusion coefficient of ethylene is about 2.2 times higher than the diffusion coefficient of 1-hexene in C_{70}. Several solute−solute and solute−C_{70} site−site pair correlation functions have been determined. Results indicate that ethylene molecules tend to form aggregates of their own in the mixture, and both ethylene and 1-hexene exhibit a tendency to reside in the vicinity of the end groups of C_{70} molecules. This aggregation may be relevant for molecules of longer chain lengths and/or with multiple branches.

We are currently simulating the effect of polymer chain lengths beyond C_{70} and polymers with multiple short-chain branches on penetrant solubilities. Furthermore, there is experimental evidence indicating an increase in penetrant solubilities due to an increase in short-chain branches in polyethylene (i.e., solubilities increase with an increase of chain end density), while the penetrant diffusion coefficients are not effected.[25]

It is important to emphasize that the results presented in this work pertain only to C_{70}. It is important to examine the molecular weight dependence of solubilities, particularly in light of the aggregate formation reported in this work. We speculate that as molecular weight increases and end concentrations decrease, the solubility of low alkanes is also likely to decrease. Furthermore, to predict solubilities in real, semicrystalline polyethylene, one must take into account the elastic effect that crystalline regions have on the solubility in the amorphous regions of the material. We are currently developing a model to predict the effects of polymer crystallinity on ethylene and 1-hexene solubilities in polyethylene. The simulation results in this work provide a good means to estimate the interaction parameters for ethylene and 1-hexene in a hypothetical amorphous polyethylene at the conditions of this work. An additional parameter is then employed to characterize the crystalline network for a specific polymeric sample.

Acknowledgments. This work is supported by the Division of Chemical Sciences, Office of Basic Energy Sciences, Office of Science, and the U.S. Department of Energy. Partial support from the Union Carbide Corporation is also gratefully acknowledged.

References and Notes

(1) Nath, S. K.; Escobedo, F. A.; de Pablo, J. J.; Patramai, I. *Ind. Eng. Chem. Res.* **1998**, *37*, 3195.
(2) Nath, S. K.; de Pablo, J. J. *J. Phys. Chem. B* **1999**, *103*, 3539.
(3) Panagiotopoulos, A. Z. *Mol. Phys.* **1987**, *61*, 813.
(4) Panagiotopoulos, A. Z.; Quirke, N.; Stapleton, M.; Tildesley, D. J. *Mol. Phys.* **1988**, *63*, 527.
(5) Laso, M.; de Pablo, J. J.; Suter, U. W. *J. Chem. Phys.* **1992**, *97*, 2817.
(6) Siepmann, J. I.; Frenkel, D. *Mol. Phys.* **1992**, *75*, 59.
(7) Escobedo, F. A.; de Pablo, J. J. *J. Chem. Phys.* **1996**, *105*, 4391.
(8) Tsang, P. C.; White, O. N.; Perigard, B. Y.; Vega, L. F.; Panagiotopoulos, A. Z. *Fluid Phase Equilib.* **1995**, *107*, 31.
(9) Liu, A.; Beck, T. L. *J. Phys. Chem. B* **1998**, *102*, 7627.
(10) Chen, B.; Siepmann, J. I. *J. Am. Chem. Soc.* **2000**, *122*, 7464.
(11) Escobedo, F. A. *AIChE J.* **2000**, *46*, 2086.
(12) Jorgensen, W. I.; Madura, J. D.; Swenson, C. J. *J. Am. Chem. Soc.* **1984**, *106*, 6638.
(13) Frenkel, D.; Smit, B. *Understanding Molecular Simulation: From Algorithms to Applications;* Academic Press: New York, 1996; pp 31−33.
(14) Allen, M. P.; Tildesley, D. J. *Computer Simulation of Liquids;* Oxford University Press: New York, 1987; pp 64−65.
(15) Nath, S. K.; Escobedo, F. A.; de Pablo, J. J. *J. Chem. Phys.* **1998**, *108*, 9905.
(16) Nath, S. K.; Banaszak, B. J.; de Pablo, J. J. *J. Chem. Phys.* **2001**, *114*, 3612.
(17) Duane, S.; Kennedy, A. D.; Pendelton, B. J.; Roweth, D. *Phys. Lett. B* **1987**, *195*, 216.
(18) Nath, S. K.; de Pablo, J. J.; DeBellis, A. D. *J. Am. Chem. Soc.* **1999**, *121*, 4252.
(19) Chapman, W. G.; Gubbins, K. E.; Jackson, G.; Radosz, M. *Ind. Eng. Chem. Res.* **1990**, *29*, 1709.
(20) Huang, S. H.; Radosz, M. *Ind. Eng. Chem. Res.* **1990**, *29*, 2284.
(21) Huang, S. H.; Radosz, M. *Ind. Eng. Chem. Res.* **1991**, *30*, 1994.
(22) Siepmann, J. I.; Martin, M. G.; Mundy, C. J.; Klein, M. L. *Mol. Phys.* **1997**, *90*, 687.
(23) Martyna, G. J.; Tobias, D. J.; Klein, M. L. *J. Chem. Phys.* **1994**, *101*, 4177.
(24) Müller-Plathe, F.; Rogres, S. C.; van Gunsteren, W. F. *Macromolecules* **1992**, *25*, 6722.
(25) Yoon, J.; Chung, C.; Lee, I. *Eur. Polym. J.* **1994**, *30*, 1209.
(26) *DIPPR Data Compilation of Pure Compound Properties;* Design Institute for Physical Properties Data; American Institute of Chemical Engineers: 1987.
(27) Reid, R. C.; Prausnitz, J. M.; Poling, B. E. *The Properties of Gases and Liquids*, 4th ed.; McGraw-Hill: New York, 1987.

MA002197L